# Normal Ultrasound Anatomy of the Skin, Nail, and Hair

**1**

Ximena Wortsman

## Contents
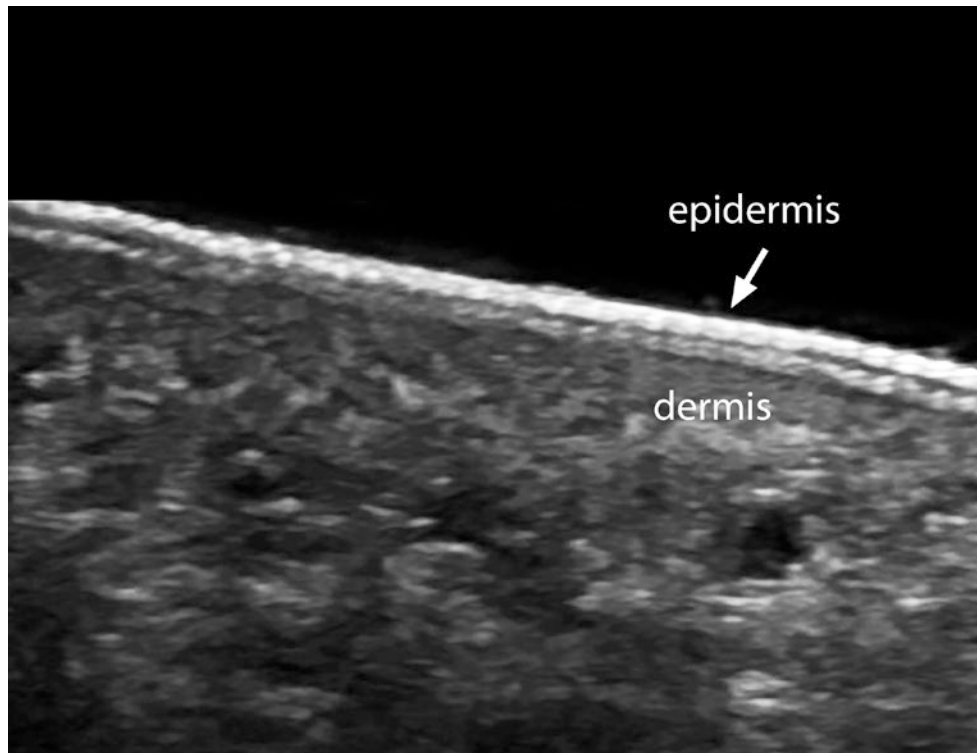
## 1.1 Ultrasound Anatomy of the Skin

The skin is composed of three layers (Fig. 1.1) [1–5]:

- The *epidermis* is the outer layer; in most regions of the body, it appears as a hyperechoic line owing to its keratin content (Fig. 1.2), but in the palmar and plantar regions (glabrous skin), the epidermis appears as a bilaminar, hyperechoic layer because of a thicker presence of keratin in the stratum corneum (Fig. 1.3).
- The *dermis* is located beneath the epidermis and appears as a hyperechoic band, less bright than the epidermis. The echogenicity of the dermis is due mainly to its collagen content. There are regional differences in the thickness of the dermis. For example, the dermis is thin in the face and ventral forearm, but thicker in the dorsal region. This variability may provide a major possibility of involvement of deeper layers in the regions that present a thinner dermis, such as the face. In photoaged skin, a subepidermal low-echogenic band (SLEB) is detected in the regions exposed to the sun; this band corresponds to the deposits of glycosaminoglycan in the upper dermis (Fig. 1.4). It should not be confused with inflammatory cutaneous diseases such as morphea.
- The *hypodermis*, also called subcutaneous tissue or subcutis, shows as a hypoechoic layer because of its fatty lobules. Between the fatty lobules are hyperechoic, linear fibrous septa.

**Fig. 1.1** Drawing of the normal anatomy of the skin.
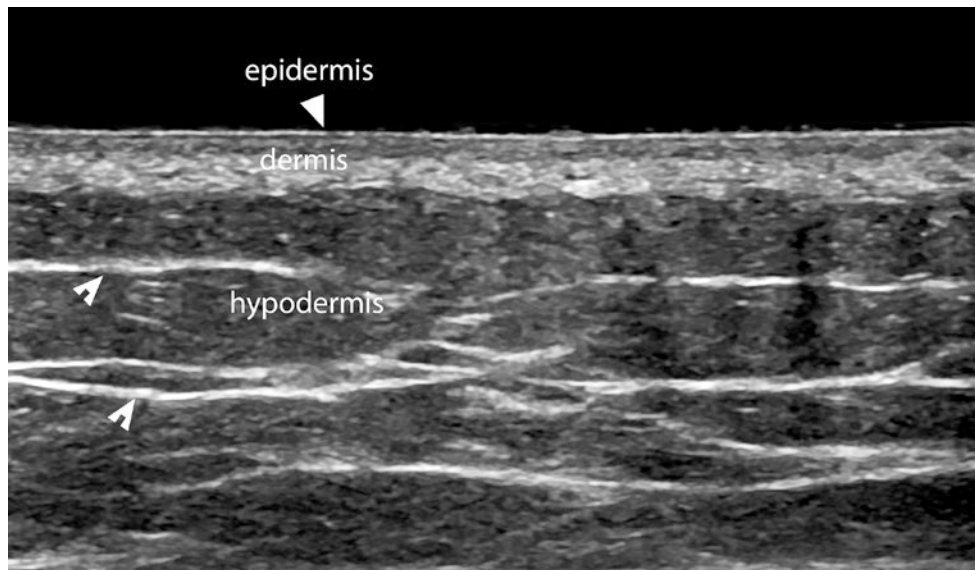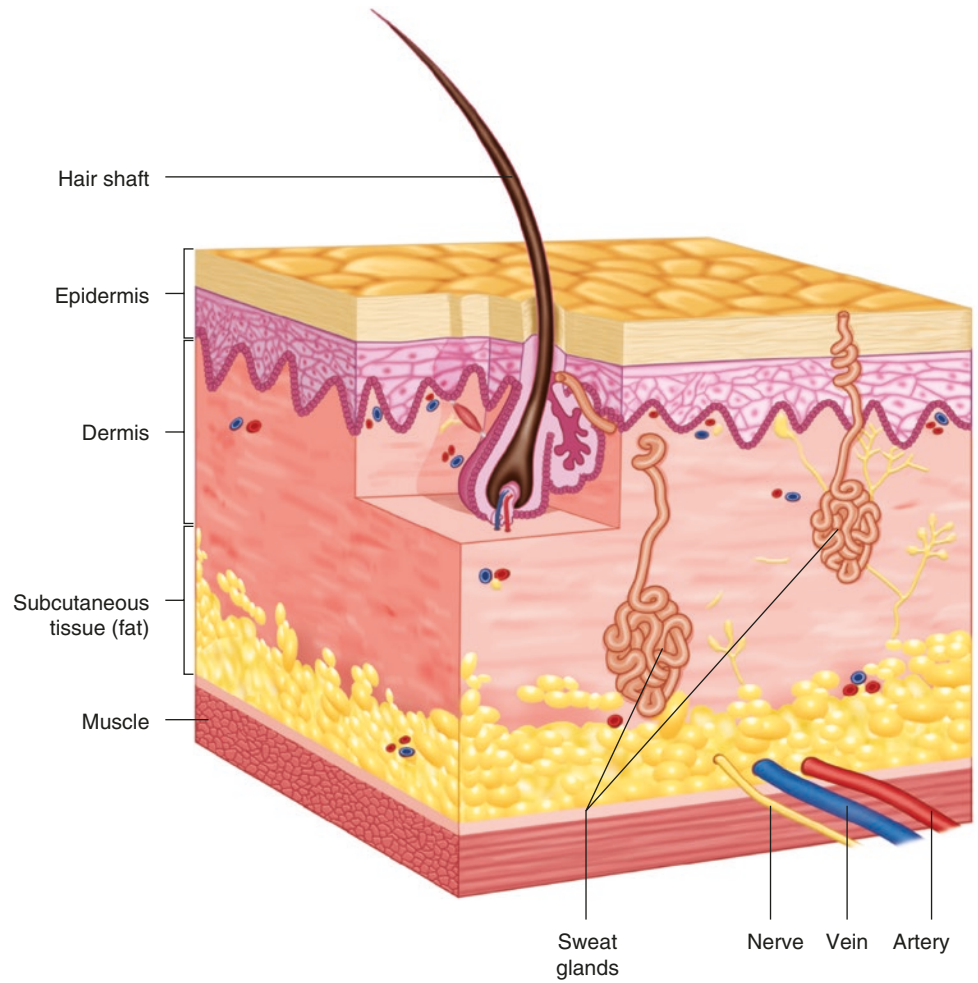


**Fig. 1.2** Normal ultrasound anatomy of the non-glabrous skin (other than the palms and soles). The *arrows* are pointing out the hyperechoic fibrous septa of the hypodermis (subcutis).

**Fig. 1.3** Normal ultrasound anatomy of the glabrous epidermis (plantar region). Notice the bilaminar hyperechoic structure of the epidermis.
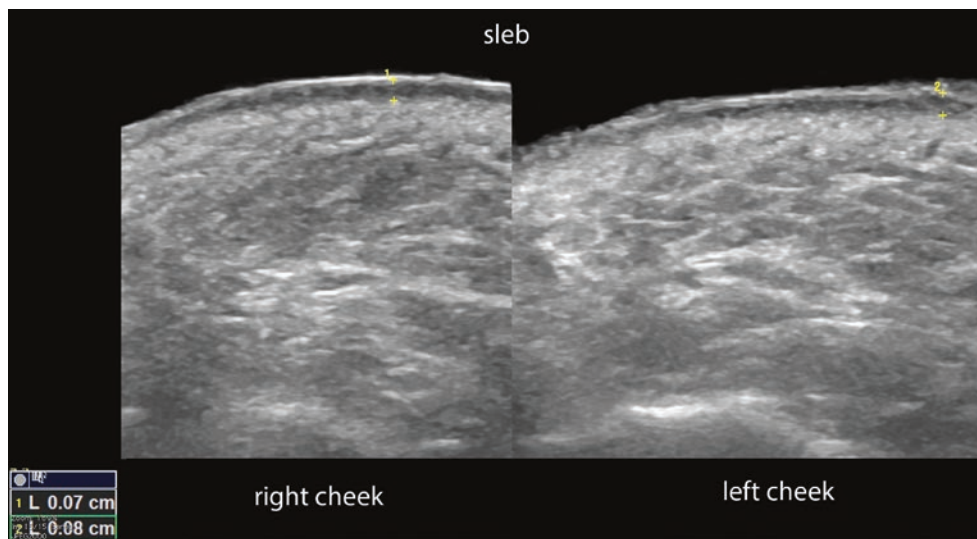


**Fig. 1.4** Subepidermal low-echogenic band, also called SLEB; between markers.

### 1.1.1 Vascularity of the Skin

Current ultrasound machines can show the hypodermal arterial and venous vessels in most corporal regions, but to detect blood flow on color Doppler, usually, a velocity of the blood of at least 2 cm/s is needed. Therefore, it is commonly not possible to detect the dermal vascularity unless there is some abnormality such as an inflammatory process, a vascular anomaly, or a tumor that increases the presence (number and/or dilatation) of vessels in this layer [1, 2, 5].

## 1.2 Ultrasound Anatomy of the Nail

The nail is composed of the nail plate, the nail bed, and the periungual regions. The *nail plate* appears as a bilaminar, hyperechoic layer with an anechoic *interplate space* in between. The outer plate is called the *dorsal plate* and the inner plate is named *ventral plate* (Figs. 1.5, 1.6, 1.7, and 1.8). The echogenicity of the nail is due to the presence of keratin, which shows different reflection capabilities of the sound waves in the periphery and center owing to variability in the density of the keratin. In machines working with higher-frequency probes (>20 MHz) the interplate space becomes more echogenic.
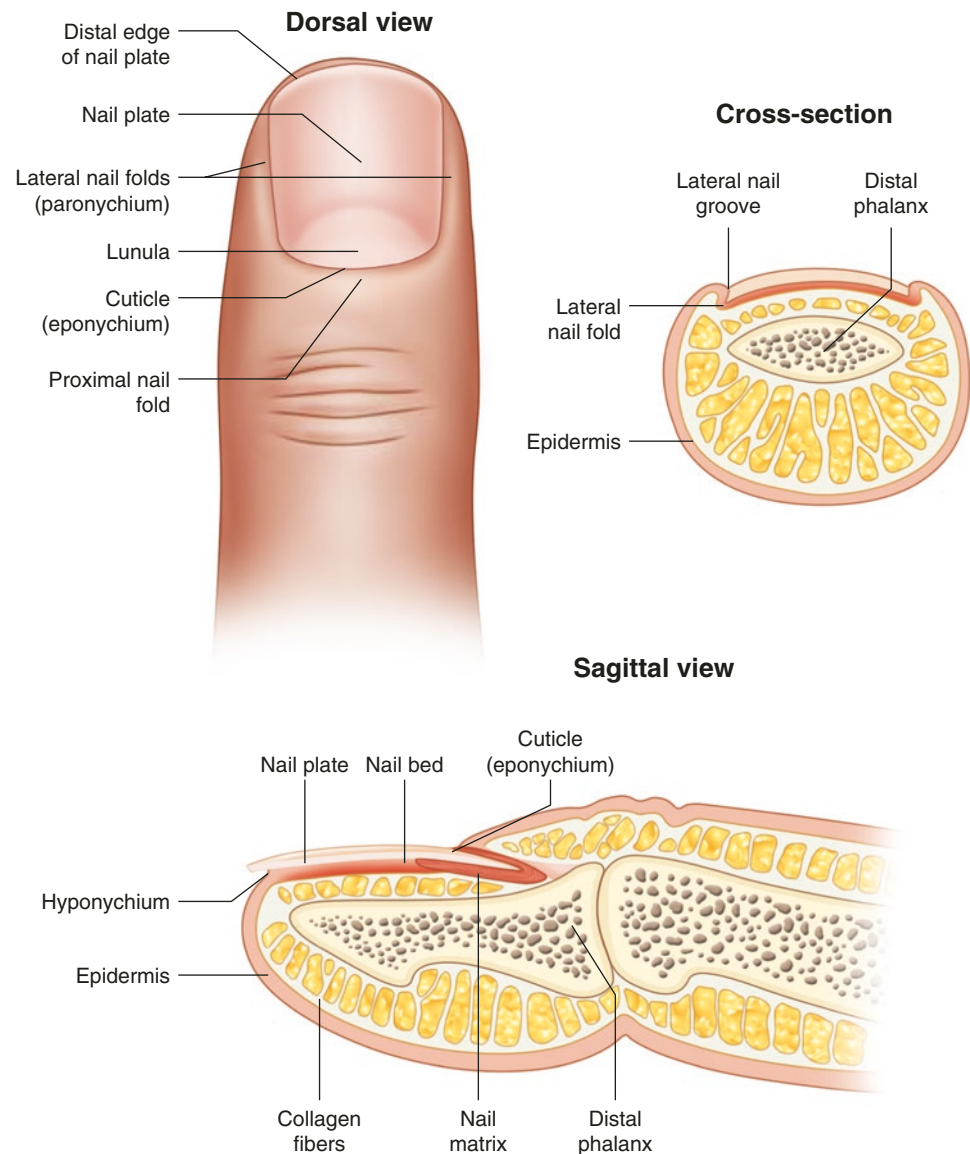
**Fig. 1.5** Drawing of the normal surface anatomy of the nail.

**Fig. 1.6** Drawing of the normal anatomy of the fingernail.

## Anatomy of the fingernail and toenail

Nail matrix  Epiphysis  Synovial membrane  Articular cartilage  Middle phalanx

Nail root
Eponychium (cuticle)
Lunula
Nail bed
Distal phalanx
Body of nail

Lateral band
Centaral tendon
} Extensor mechanism

Flexor digitorum superficialis tendon

Fibrous tendon sheath of finger

Synovial (flexor tendon) sheath of finger

Flexor digitorum profundus tendon

Palmar ligament (plate)

Articular cavity

Nerves   Arteries   Septa

Distal anterior closed space (pulp)

**Fig. 1.7** Normal anatomy of the toenail in cross section.

## Cross section of toenail

Dorsal nail plate
Ventral nail plate
Fibrous attachment of bone

Nail bed
Eponychium
Lateral nail groove
Bone of finger
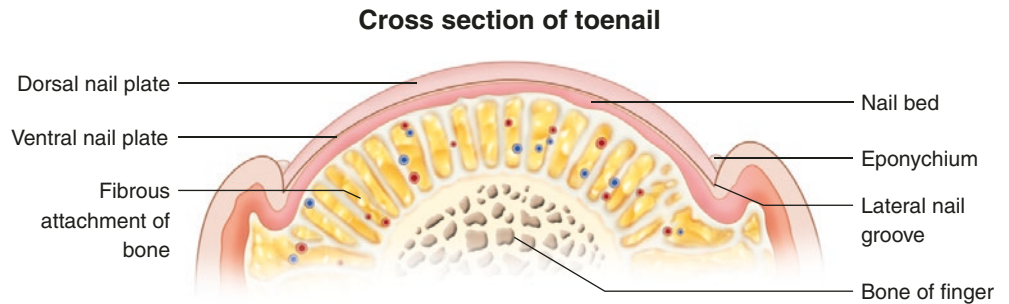
**Fig. 1.8** Normal ultrasound anatomy of the nail (longitudinal view).



dorsal plate
proximal nail fold
ventral plate
nail bed
matrix region
distal phalanx bony margin
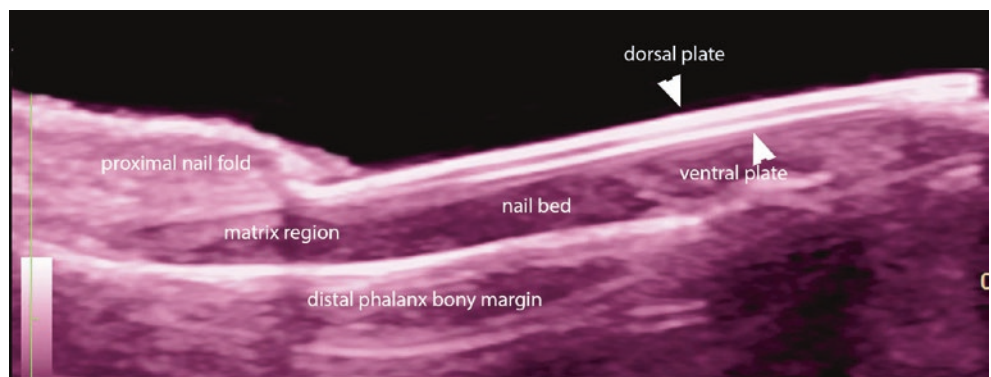
The nail bed shows as a hypoechoic space that usually turns slightly more hyperechoic in the proximal part, where the matrix is located. The periungual region is mainly composed of hyperechoic dermis and is separated in the proximal and lateral nail folds.

There is a close relationship between the nail unit and the distal insertion of the extensor tendon and the distal interphalangeal joint. Thus, on histology, some fibers of the extensor tendon have been seen to reach the proximal part of the nail unit. This can explain why tendinous and distal joint conditions can easily affect the ungual or periungual regions [1, 2, 6–9].

### 1.2.1  Vascularity of the Nail

The blood flow comes from the digital arteries on both sides of the fingers, and with the current machines, the vascularity can be detected in the inner two-thirds of the nail bed, mostly close to the bony margin of the distal phalanx. Usually, if on ultrasound the blood flow touches the ventral plate, we consider the presence of some abnormality that stimulates an increase in the number or dilatation of the vessels (Fig. 1.9) [1, 2, 6–9].
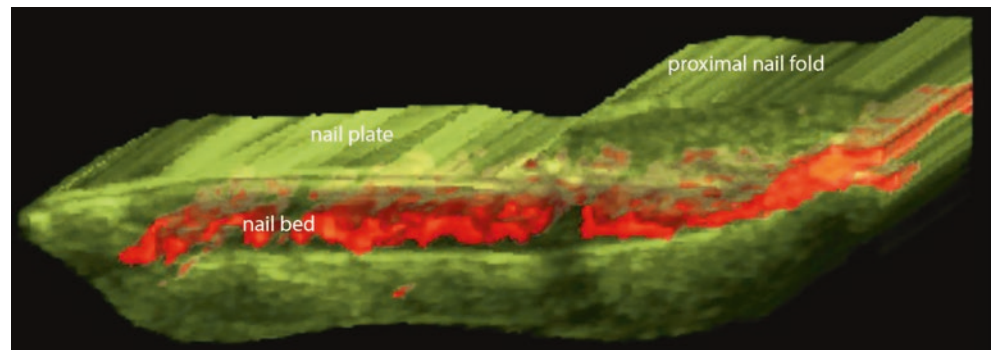


**Fig. 1.9** 3D Color Power Doppler reconstruction of the nail blood flow (longitudinal view).

## 1.3    Ultrasound Anatomy of the Hair

The hair is composed of two parts: the hair follicle and the hair tract or shaft. The *hair follicles* appear on ultrasound as hypoechoic, oblique bands located in the dermis and sometimes the upper hypodermis. The degree of obliquity of the hair follicles can vary according to ethnic factors and the type of hair. For example, individuals with curly hair show more oblique follicles than persons with straight hair, in whom the hair follicles tend to be more vertical (Figs. 1.10 and 1.11).
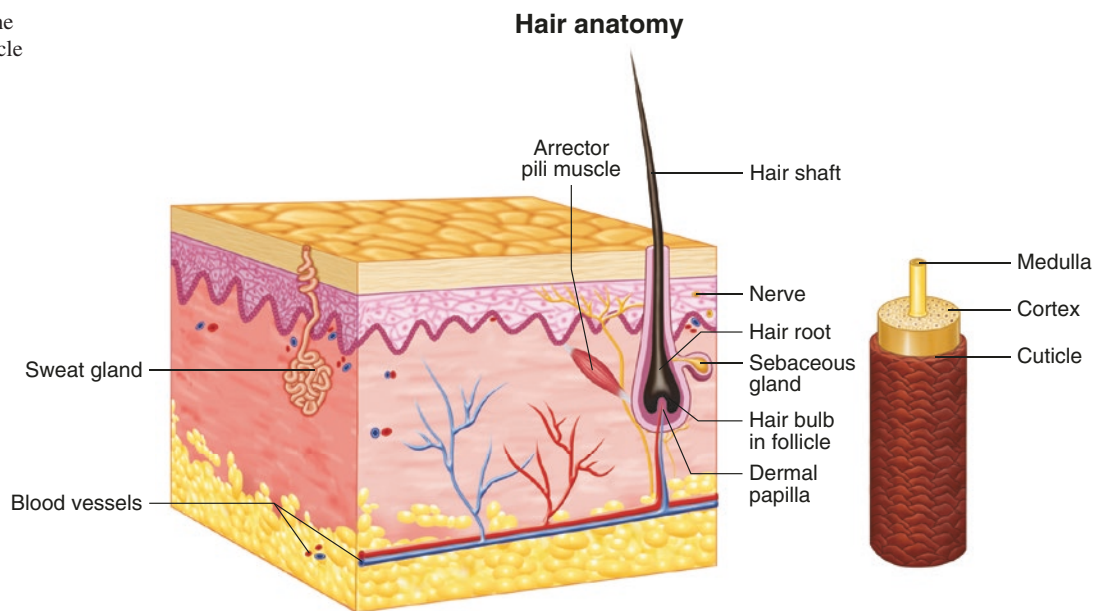
The *hair cycle* may be seen on ultrasound (Fig. 1.12). For example, in the *telogen* or resting phase, the hair follicles are seen as tiny, hypoechoic, oval-shaped structures located in the upper dermis, usually in the subepidermal region. In the *anagen* or mature phase, a fully developed hair follicle is detected in the upper and lower dermis and sometimes the upper hypodermis. In the *catagen* or intermediate phase, the hair follicles are between the telogen and anagen locations.

Monitoring of the hair cycle may be useful in some hair disease conditions such as telogen effluvium.

The *hair tracts or shafts* appear as laminar, hyperechoic structures because of their keratin content. The scalp hair tracts show two types morphology (Fig. 1.13). Most (approximately 80%) present as a trilaminar, hyperechoic structure that corresponds to the terminal hair, showing an outer cuticle-cortex complex and an inner medulla. The rest of the scalp hair tracts and most hair tracts of the body present as a bilaminar, hyperechoic structure that corresponds to the villus type of hair. A higher proportion of bilaminar vellus hair in the scalp may indicate the presence of an abnormality in the generation of the hair, such as androgenetic alopecia. This vellus, bilaminar type of hair seems to be more fragile than the trilaminar type.

The eyelashes and eyebrows commonly appear in machines working with probes ≤20 MHz as a monolaminar hyperechoic structure, perhaps because of a thinner layer of keratin but these may show a bilaminar appearance on higher frequencies [1, 10, 11].

**Fig. 1.10**  Drawing of the anatomy of the hair follicle and terminal hair tract.



**Hair anatomy**

Arrector pili muscle
Hair shaft
Nerve
Hair root
Sebaceous gland
Hair bulb in follicle
Dermal papilla
Sweat gland
Blood vessels
Medulla
Cortex
Cuticle

**Fig. 1.11** Normal ultrasound anatomy of the hair follicles. (**a**) Greyscale at 18 MHz (*arrowheads*). (**b**) Greyscale at 70 MHz (*arrows*).
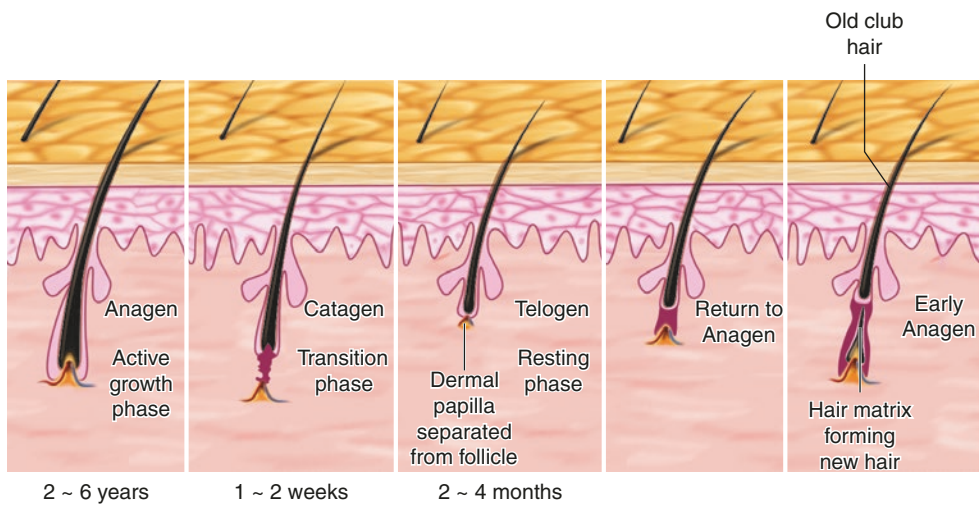
**Fig. 1.12** Drawing of the hair cycle.
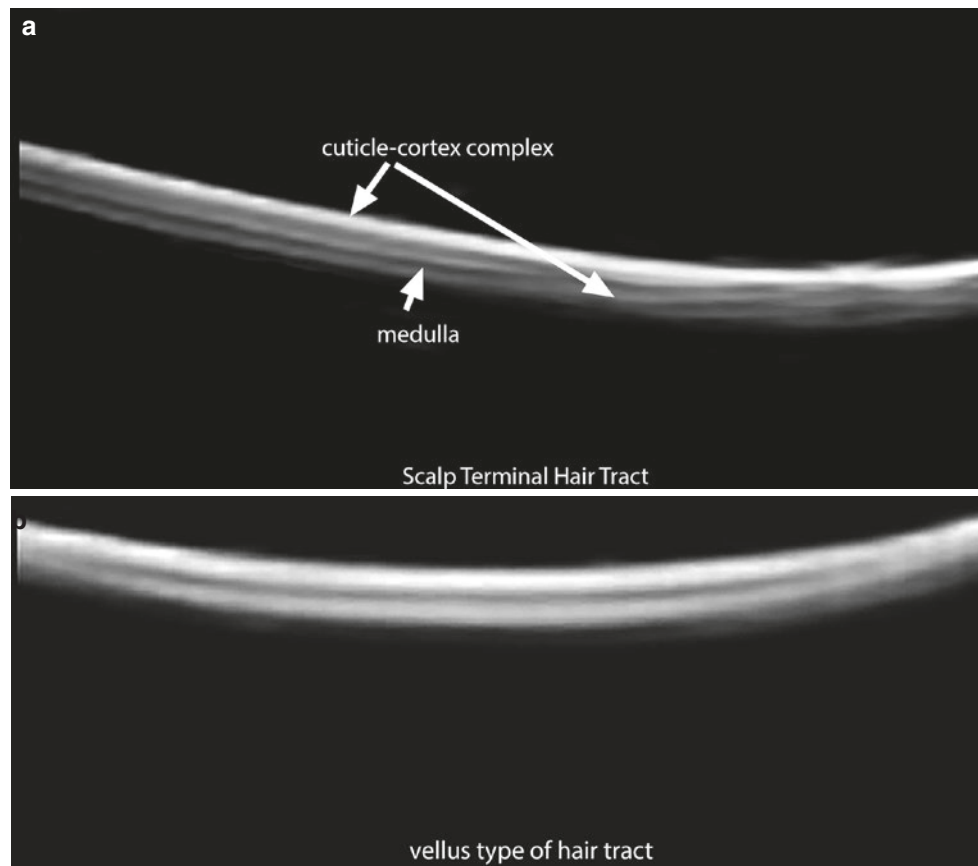
**Fig. 1.13** Normal ultrasound morphology of the hair tracts. (**a**) Trilaminar terminal hair tract of the scalp. (**b**) Bilaminar or vellus type of hair without medulla most commonly found in the rest of the body.

## 1.4    Structures Adjacent to the Skin

### 1.4.1    Lymph Nodes

Lymph nodes appear on ultrasound as well-defined, oval-shaped structures with a thin, hypoechoic band that corresponds to the cortex and a hyperechoic medulla in the central part. The vascularity is commonly seen in the center (centripetal) or in one of the borders of the lymph node at the point of entrance of the hilum vessels (Fig. 1.14). By convention, the normal size of the lymph node is maximum 1 cm in transverse view, but larger lymph nodes may be detected that can reach 2 cm in transverse view in the jugulodigastric, axillary, and groin regions. The location of the lymph nodes follows the anatomical chains of drainage of the lymphatic system. Inflammatory lymph nodes are usually larger and present a thicker cortex but tend to retain their oval shape and centripetal vascularity. Suspicious signs of malignancy can include a change in shape (from oval to round); in size (larger than 1 cm); in echogenicity (loss of the difference between the cortex and the medulla, becoming fully hypoechoic); in the appearance of hypoechoic, eccentric nodules in the cortex or medulla; and the appearance of mostly cortical vascularity with irregular and tortuous vessels [1] (See Chap. 5).
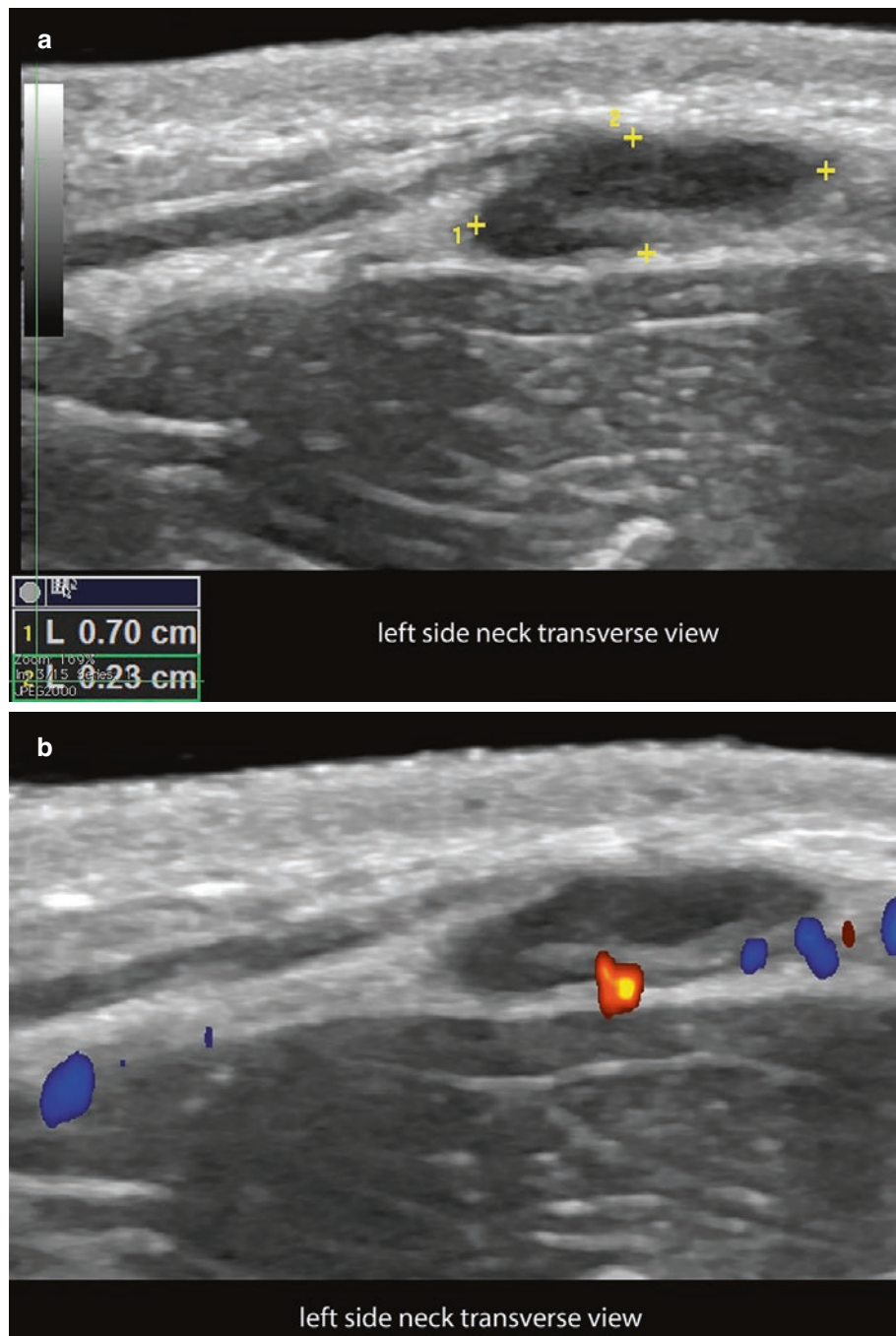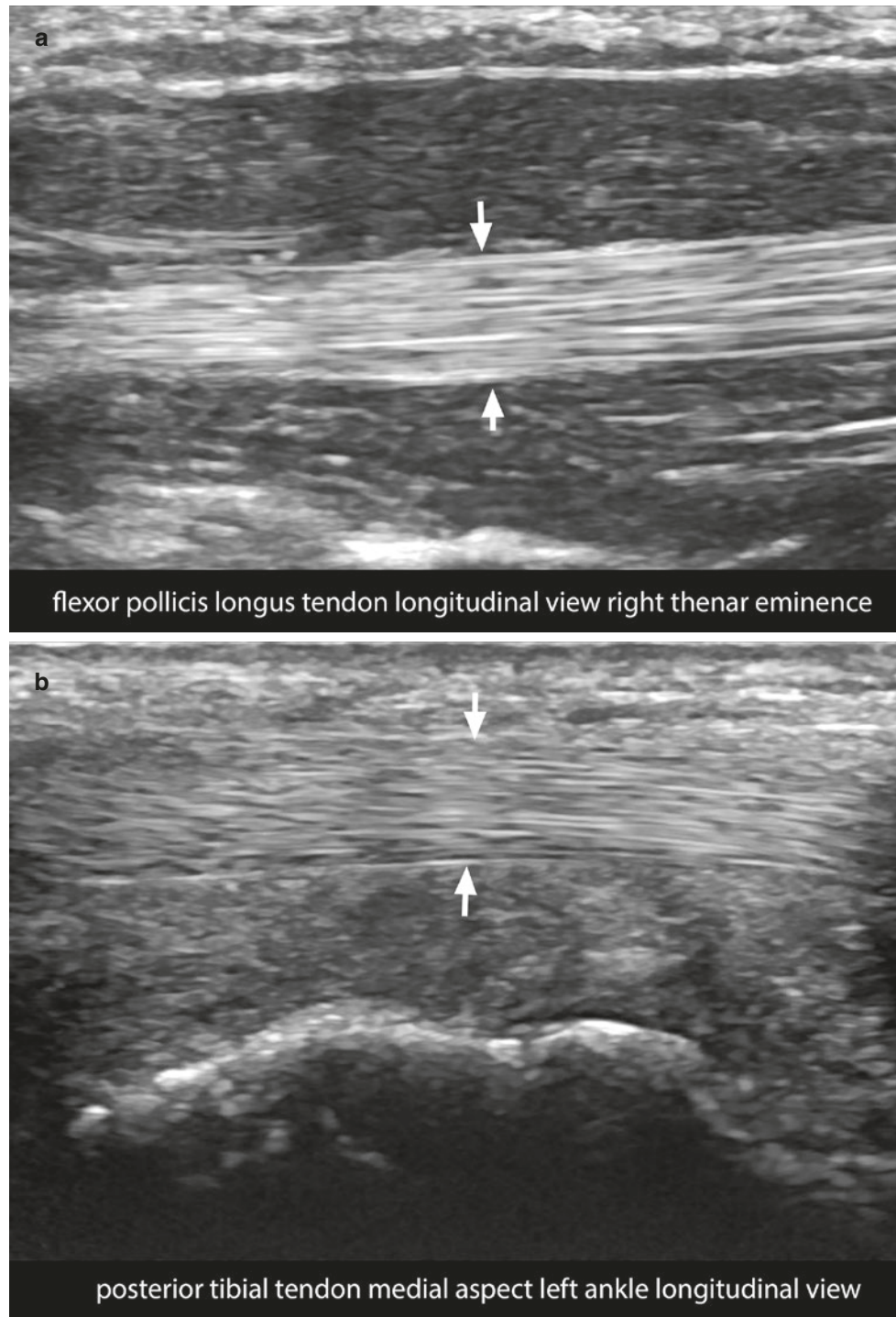
**Fig. 1.14** Normal ultrasound anatomy of the lymph node (transverse views; left side of the neck). (**a**) Greyscale (between markers). (**b**) Color Doppler (transverse view). Notice the normal size (0.7 cm transverse axis), the oval shape, the hypoechoic band of the cortex, and the hyperechoic center of the medulla. On color Doppler, the vascular hilum is located at the deep border.

## 1.4.2   Tendons

The tendons appear as hyperechoic, fibrillary structures, as their structure is formed by parallel bundles of collagen surrounded by a virtual synovial sheath in most body regions (Fig. 1.15). There are tendons, such as the Achilles tendon, that show a virtual paratenon instead of a synovial sheath.

Tendons and their synovial sheath can become inflamed in some rheumatic diseases that may also present skin lesions. Tendons can also present tendinopathy (i.e., chronic alteration of their fibrillar pattern) in some dermatologic diseases such as psoriasis. During the dynamic study, it is possible to detect real-time tendinous movements such as for example during flexion and extension [1, 12].

flexor pollicis longus tendon longitudinal view right thenar eminence

posterior tibial tendon medial aspect left ankle longitudinal view

**Fig. 1.15** Normal ultrasound morphology of the tendons. (**a**) Flexor pollicis longus. (**b**) Posterior tibial tendon. Notice the hyperechoic fibrillary pattern of the tendons (*arrows*).

## 1.4.3 Muscle

The muscles appear as hypoechoic, fibrillary structures that present dynamic changes under contraction and rest (Fig. 1.16). There are accessory muscles that show as normal variants in certain anatomical locations, such as the extensor digitorum brevis muscle in the hand (Fig. 1.17), the anconeus muscle in the posterior aspect of the elbow, and the peroneus quartus muscle in the ankle. These accessory muscles may simulate dermatologic or soft tissue masses. Table 1.1 lists the most common accessory muscles and their location in the limbs [1, 13].



right lateral gastrocnemius muscle longitudinal view

**Fig. 1.16** Normal ultrasound morphology of the muscle (lateral gastrocnemius; *arrows*).



extensor digitorum brevis dorsum left hand  longitudinal view

**Fig. 1.17** Ultrasound morphology of an accessory muscle at the dorsum of the left hand: extensor digitorum brevis (*arrowheads*).

**Table 1.1** Frequent accessory muscles of the limbs

| Accessory muscles | Location |
|---|---|
| Chondroepitrochlearis | Arm |
| Anconeus | Elbow |
| Anomalous palmaris longus | Forearm |
| Proximal origin lumbrical muscles | Wrist and hand |
| Extensor digitorum brevis | Wrist and hand |
| Flexor digitorum superficialis of the index | Wrist and hand |
| Abductor digiti minimi | Wrist and hand |
| Tensor fasciae suralis | Knee |
| Accessory soleus | Ankle |
| Peroneus quartus | Ankle |
| Accessory flexor digitorum longus | Ankle |

### 1.4.4 Nerves

Nerves present as fascicular structures with a mixed hyperechoic and hypoechoic pattern. In transverse view, they appear as oval-shaped, hyperechoic structures with multiple hypoechoic dots, and may resemble the ultrasound appearance of an ovary.

Nerves can show anatomical variants; one of the most commonly seen is the bifid median nerve in the wrist (Fig. 1.18), which can present with a remnant artery between the two neural branches, called *persistent median artery*. Sometimes this remnant artery can become thrombosed, and the patient may present a swelling in the palmar aspect of the wrist [1].

left median nerve longitudinal view

1 L 0.42 cm
2 L 0.17 cm

bifid median nerve right wrist transverse view
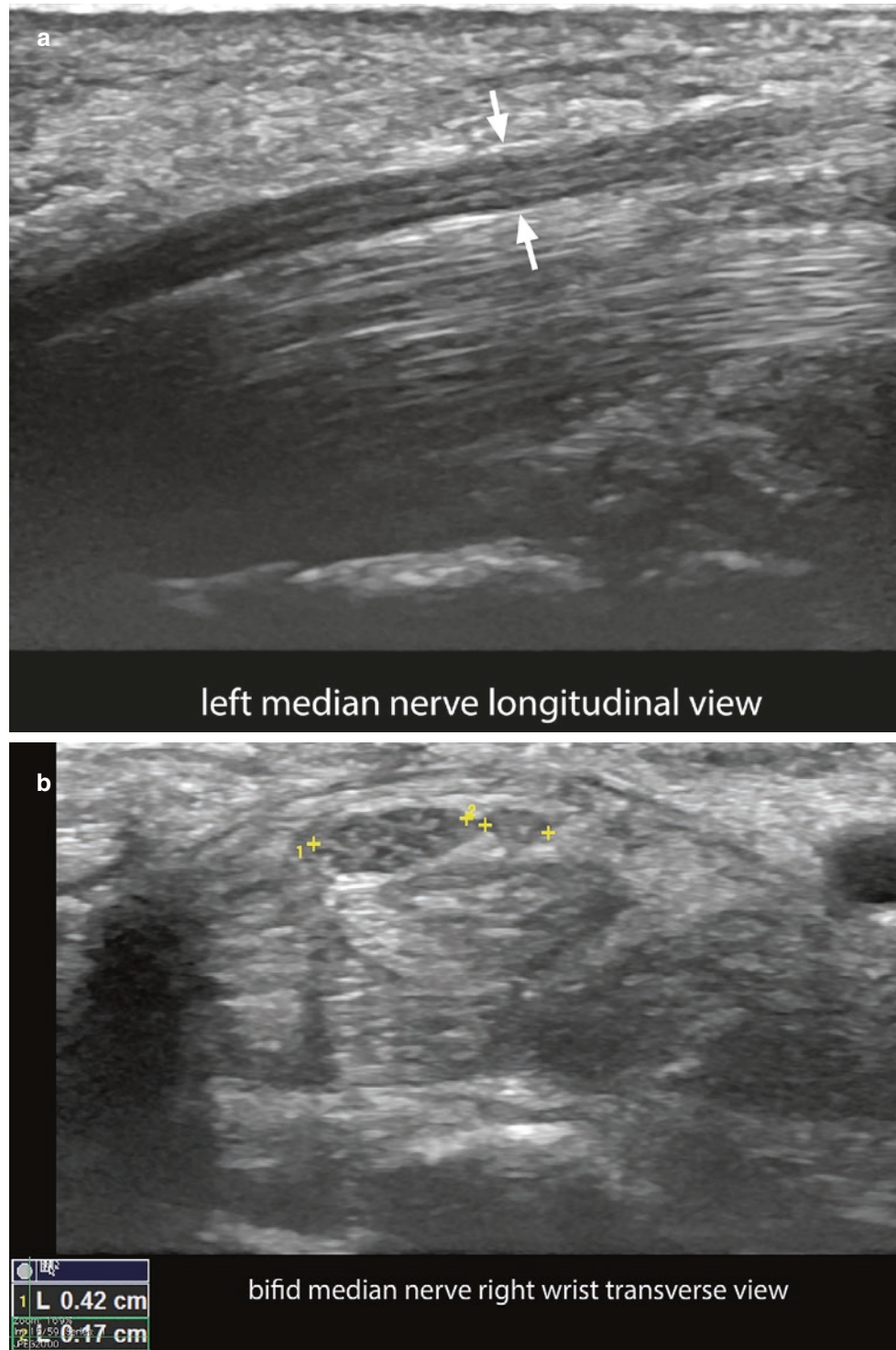
**Fig. 1.18** Normal ultrasound morphology of the nerves. (**a**) Median nerve (longitudinal view; *arrows*) shows the fascicular pattern of the nerve. (**b**) Bifid variant of the median nerve at the wrist (between markers; transverse view) demonstrates two branches with fascicular pattern in the carpal tunnel, one of them dominant, with larger size (0.42 cm vs. 0.17 cm; transverse axis in (**b**)).

## 1.4.5    Bursae

Bursae are virtual sac-like subcutaneous structures located in areas exposed to high friction, such as the plantar or posterior elbow regions. Normally, bursae are not detected, but in the presence of inflammation they show as anechoic, fluid-filled, and compressible structures with echoic synovium, which in some cases can be very prominent (Fig. 1.19). Bursae can also be generated "de novo" or acquired in rarer anatomical locations such as the fingers, toes, or the malleolar regions through high exposure to friction. The latter condition is called *adventitial bursitis*. Table 1.2 lists common bursae and their anatomical locations [1, 14].

**Fig. 1.19** Ultrasound morphology of bursitis. (**a**) Olecranon bursitis (greyscale with color filter; longitudinal view) shows anechoic fluid and prominent synovium (bursa; *arrows*) in the hypodermis of the posterior aspect of the left elbow. (**b**) Plantar bursitis (greyscale; longitudinal view; plantar region) shows anechoic fluid and prominent synovium (bursa between markers) located on top of the flexor tendon of the first toe.

olecranon bursa posterior aspect left elbow longitudinal view

plantar bursa right first toe longitudinal view
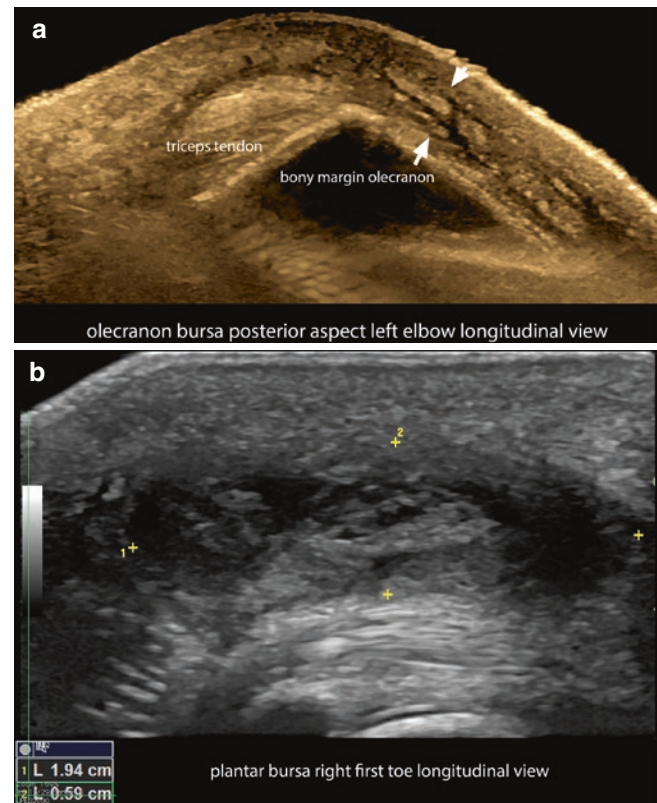
**Table 1.2** Frequent bursae locations

| Bursae | Location |
| --- | --- |
| Olecranon | Posterior elbow |
| Lumbar Baastrup's | Interspinous processes |
| Trochanteric | Hip |
| Prepatellar | Anterior knee |
| Infrapatellar | Anterior knee |
| Tibial tuberosity | Anterior knee |
| Calcaneal | Posterior ankle |
| Distal metatarsal | Plantar region |

### 1.4.6   Cartilage

The cartilage appears in ultrasound as hypoechoic bands, usually without detectable vascularity. These anatomical characteristics are seen in the nasal cartilages (superior and alar) and the ear pinna cartilage (Fig. 1.20). In the auricular region, the cartilage is detected in the upper two thirds, but the lobule of the ear pinna does not contain cartilage [1, 15].
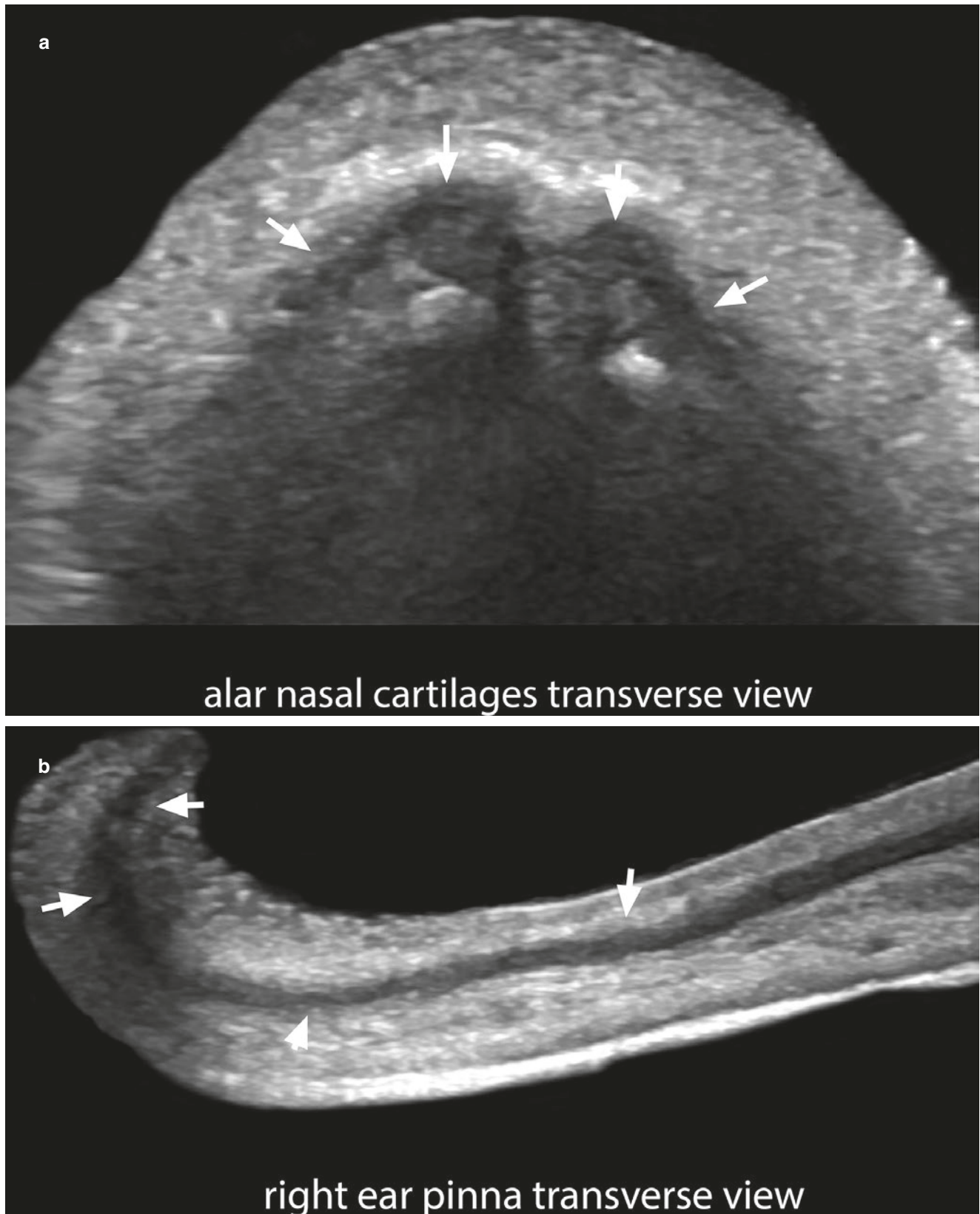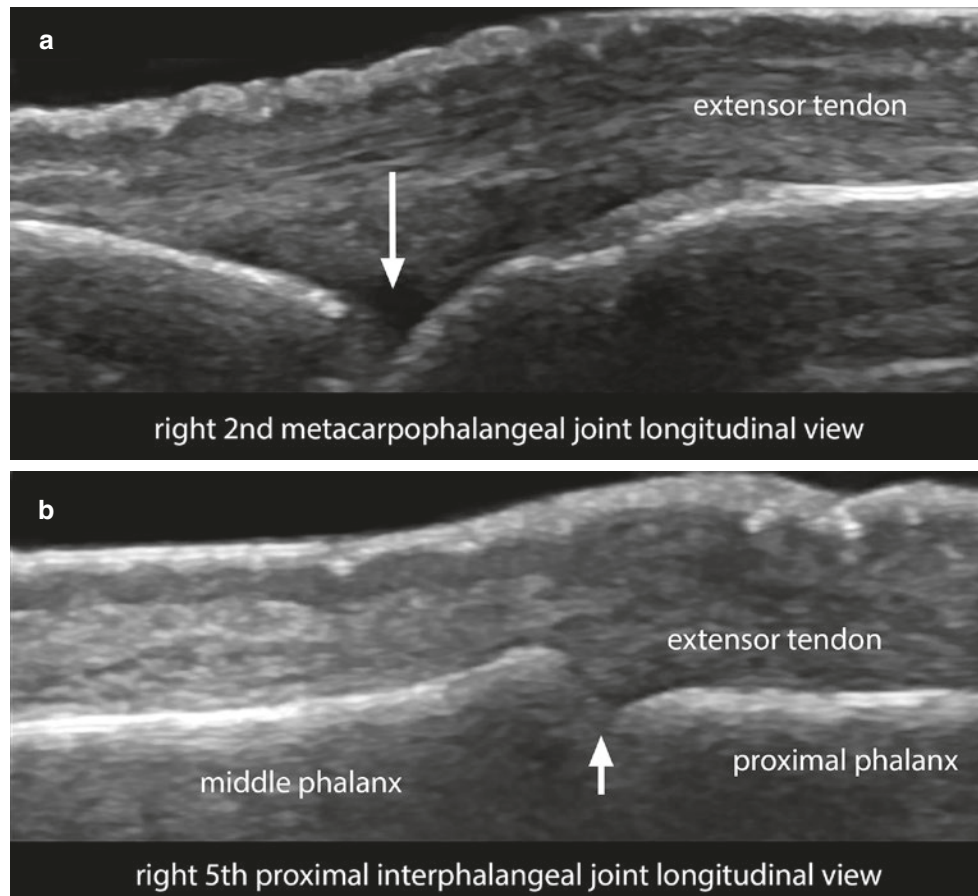
**Fig. 1.20** Normal ultrasound morphology of the cartilage (greyscale; transverse views). (**a**) Alar nasal cartilages (*arrows*) at the tip of the nose. (**b**) Auricular cartilage (*arrows*) of the right ear pinna. Notice the hypoechogenicity of the cartilage pattern.

### 1.4.7   Joints

The joint spaces contain hypoechoic synovial cartilage on top of the epiphyseal parts of the long bones; a laminar anechoic band of fluid may be detected. Normally, the fluid of the joint does not displace the tendons upward, so if this situation is detected, a synovitis should be suspected. In nor- mal conditions, there is no vascularity within the joint space, and the vascularity in the periphery of the joint corresponds to the normal digital vessels. If vascularity starts to surround the joint or appears within the synovium, a more severe stage of synovitis is suspected. The margins of the bony cortex appear as hyperechoic lines with posterior acoustic shadow- ing due to the calcium content (Fig. 1.21) [1, 16].



**Fig. 1.21**   Normal ultrasound morphology of the joints (longitudinal views). (**a**) Metacarpophalangeal joint in the right second finger. (**b**) Proximal interphalangeal joint. The *arrows* are pointing out the joint spaces.

### 1.4.8 Vessels

Arteries and veins appear as anechoic tubular structures with a variable thickness according to the anatomical location.

Veins are commonly compressible with the probe and may be easily collapsed and dilated. The spectral curve analysis shows the systolic and diastolic phases in the arteries, and a monophasic type of flow in the veins (Figs. 1.22 and 1.23).

**Fig. 1.22** Arterial blood flow spectral curve analysis. Notice the systolic and diastolic peaks. (**a**) Normal right temporal artery (peak systolic velocity, 61 cm/s). (**b**) A variant, caliber-persistent artery in the lower lip (transverse view), shows high peak systolic velocity, 75 cm/s
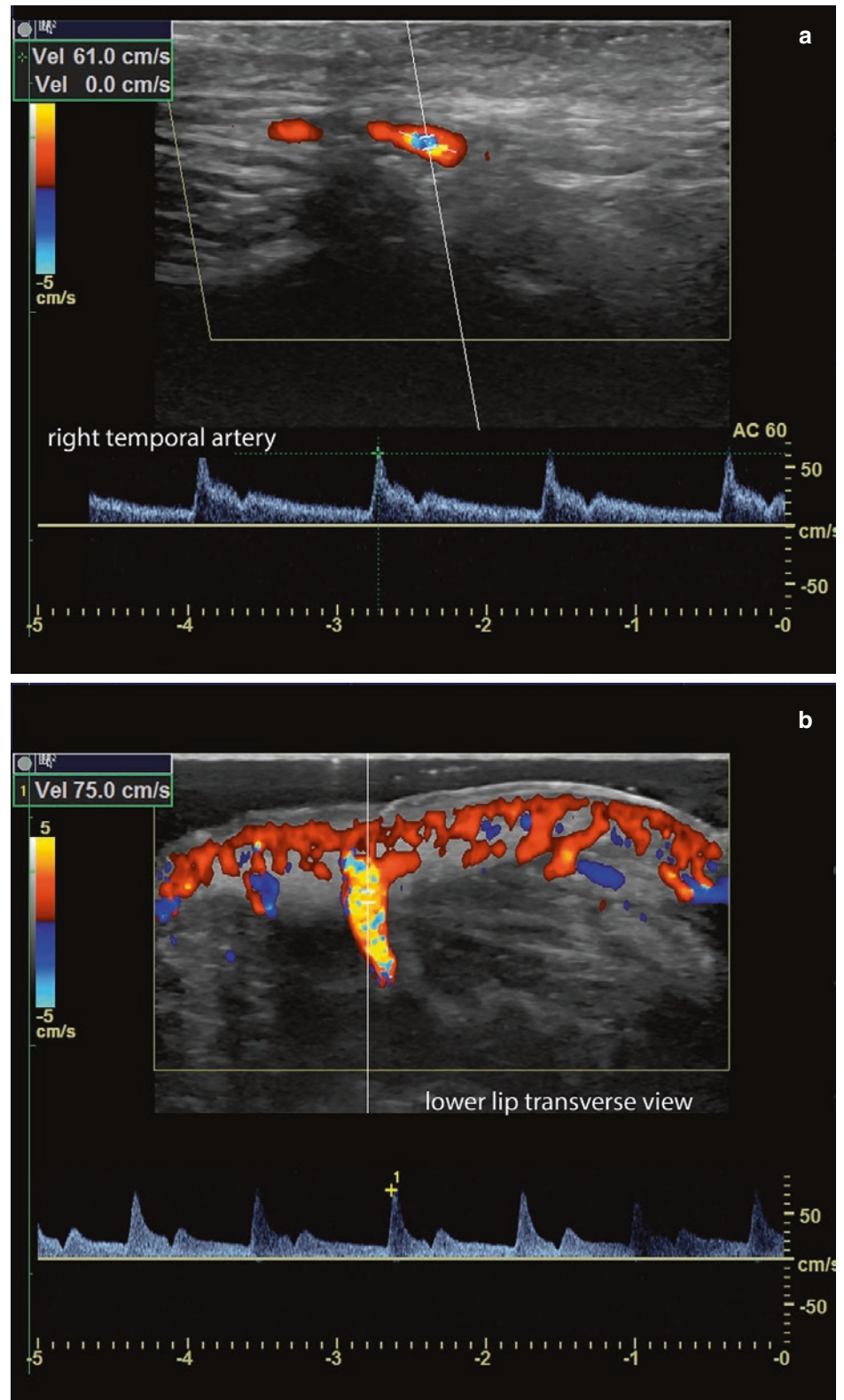
Anatomical variants in the presence, number, and location of the vessels can be recognized in the different regions of the body [1]. For example, a variant called *caliber-persistent artery* in the lip (an artery that does not decrease in size as usual when entering the labial dermis) may simulate a tumor [17, 18]. The velocity of the blood flow varies according to the size and type of the vessel. Usually in the hypodermis, the vessels present a velocity of 15 cm/s or less [1].
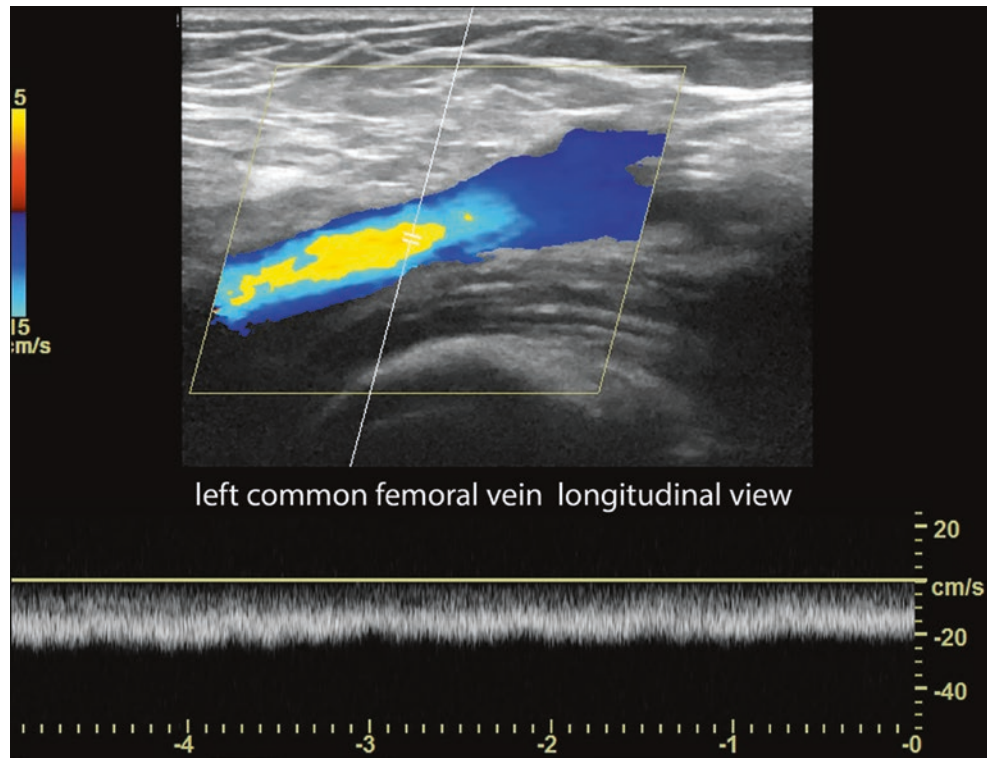


**Fig. 1.23**  Venous blood flow spectral curve analysis demonstrates a monophasic flow at the left common femoral vein.
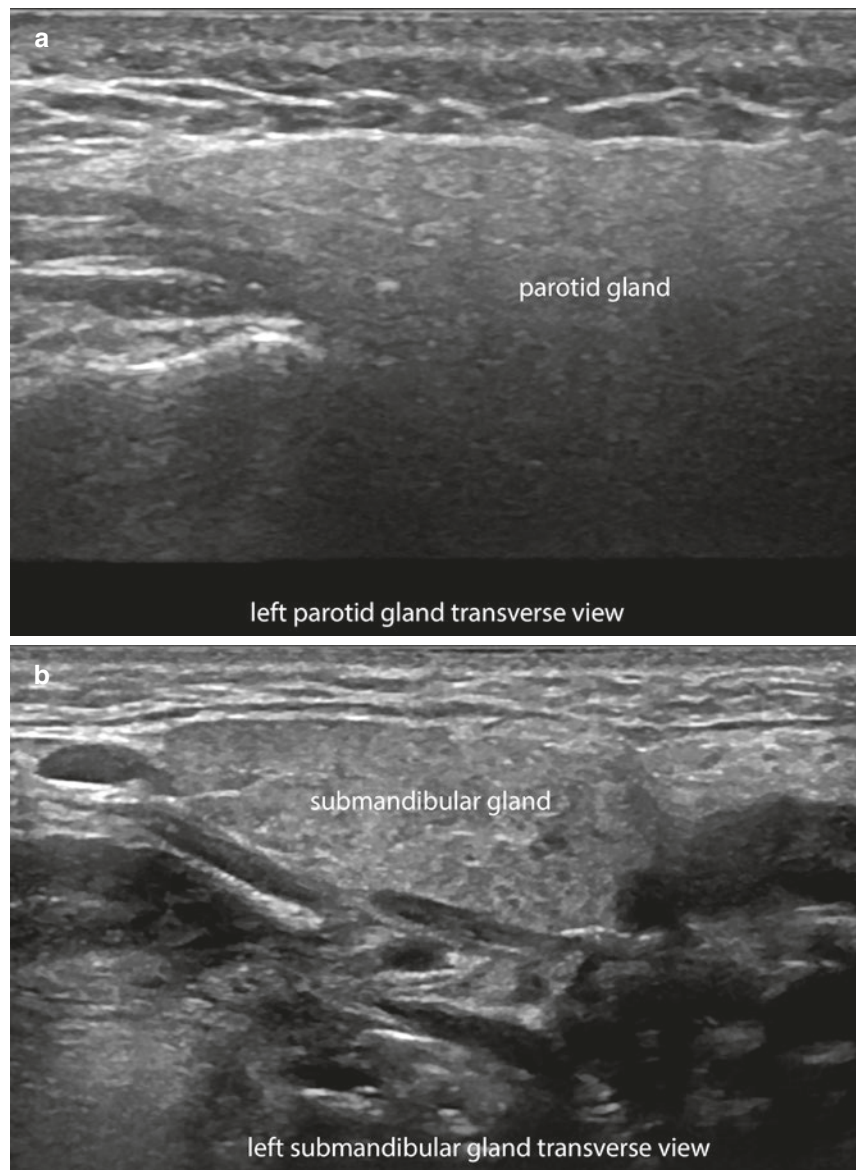
### 1.4.9 Salivary Glands

The major salivary glands are the parotid and submandibular glands. However, there are also several minor salivary glands located in the submucosal region of the lips. The parotid and submandibular glands are hyperechoic in comparison with the muscles in the vicinity. The minor salivary glands are hypoechoic (Fig. 1.24).

In the parotid region, there are frequent anatomical gland variants, such as a prominent ventral part of the parotid gland that lies on top of the upper segment of the masseter muscle (Fig. 1.25), and an accessory parotid gland that also is located on top of the masseter muscle but is separated from the main parotid gland.

The submucosal minor salivary glands located in the oral mucosa appear as well-defined, round, hypoechoic structures. These glands can be normally prominent in some individuals or may become inflamed and simulate a mucocele or a tumor [1].

Fig. 1.24 Ultrasound morphology of salivary glands. (**a**) Parotid gland (transverse view). (**b**) Submandibular gland (transverse view). (**c**) Minor salivary submucosal gland at the lower lip (between markers; longitudinal view). Notice the homogeneity of the glands, mostly hyperechoic in the parotid and submandibular glands and hypoechoic in the minor salivary glands.

**Fig. 1.24** (Continued)



minor salivary gland lower lip longitudinal view



parotid gland

masseter muscle

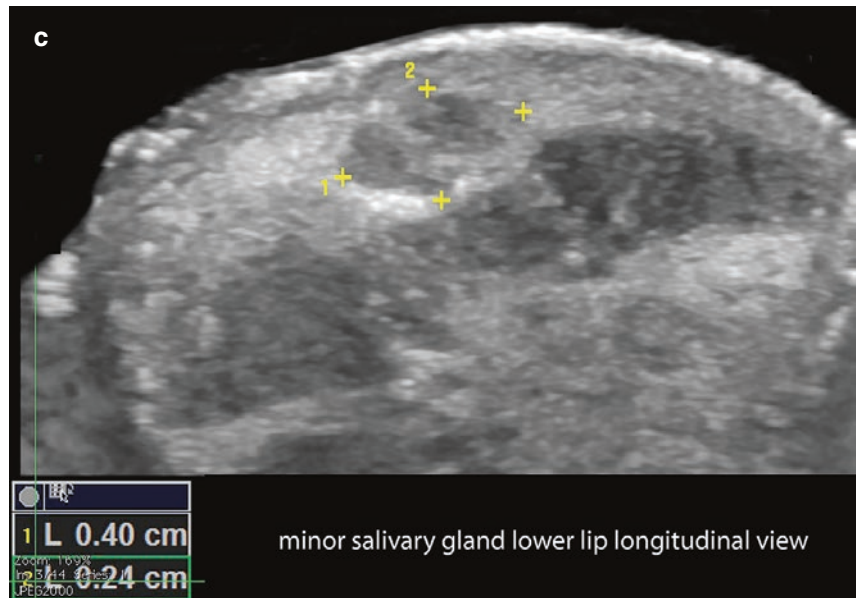right parotid gland covering the masseter muscle transverse view

**Fig. 1.25** An anatomical variant shows a prominent ventral part (*asterisks*) of the parotid gland which covers the upper part of the masseter muscle.
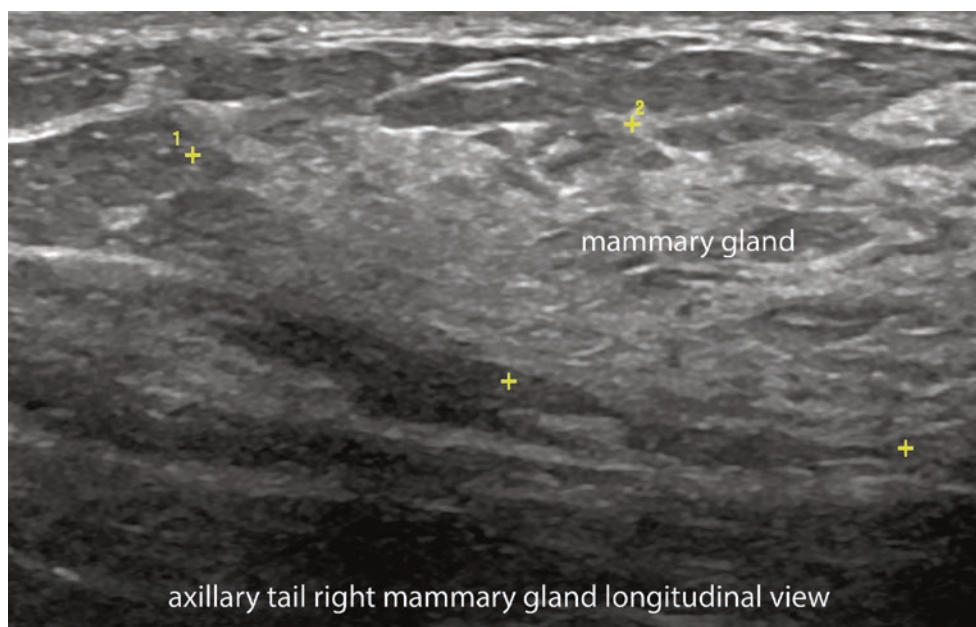
## 1.5  Mammary Glands

The fibroglandular mammary tissue can be seen as a mixed hyperechoic and hypoechoic structure. The mammary gland presents an axillary tail that goes to the base of the axillary region. In some patients, the axillary tail can be prominent (Fig. 1.26). Beneath the hypoechoic structure of the nipple, there are anechoic tubular ducts, which correspond to the location of the drainage of the ductal mammary system. The dermis of the areola contains small accessory glands, called *Montgomery glands*, that sometimes may become inflamed and simulate a dermatologic nodule. The ectopic presence of mammary tissue (for example, isolated in the upper part of the axillary region), the development of fibroglandular mammary tissue in men (gynecomastia), or the presence of the breast

buds may also mimic a soft tissue tumor. Rarely, an ectopic or supernumerary nipple may be detected, which usually follows the location of the embryonic milk mammary lines [1, 19].

### 1.5.1  Bone/Calcium

On ultrasound, only the cortex of the bone can be detected because the sound is stopped by the calcium. It appears as a hyperechoic line with posterior acoustic shadowing artifact, as seen in Fig. 1.21. Calcium deposits show as hyperechoic spots or bands, according to their origin. For example, calcinosis deposits present as hyperechoic spots, and bony implants present as hyperechoic bands. These calcium deposits usually present a posterior acoustic shadowing artifact according to their size [1, 20].



**Fig. 1.26**  Normal ultrasound morphology of the tail of the mammary gland at the base of the axillary region (between markers; longitudinal view).

# References

1. Wortsman X, Wortsman J, Carreño L, Morales C, Sazunic I, Jemec GBE. Sonographic anatomy of the skin, appendages and adjacent structures. In: Wortsman X, Jemec GBE, editors. Dermatologic ultrasound with clinical and histologic correlations. New York: Springer; 2013. p. 15–35.
2. Wortsman X. Common applications of dermatologic sonography. J Ultrasound Med. 2012;31:97–111.
3. Farinelli N, Berardesca E. The skin integument: variation relative to sex, age, race, and body region. In: Serup J, Jemec GBE, Grove GL, editors. Handbook of noninvasive methods and the skin. 2nd ed. Boca Raton: Taylor & Francis; 2006. p. 27–36.
4. Sharman AM, Kirmi O, Anslow P. Imaging of the skin, subcutis, and galea aponeurotica. Semin Ultrasound CT MR. 2009;30:452–64.
5. Wortsman X, Wortsman J. Clinical usefulness of variable frequency ultrasound in localized lesions of the skin. J Am Acad Dermatol. 2010;62:247–56.
6. Cecchini A, Montella A, Ena P, Meloni GB, Mazzarello V. Ultrasound anatomy of normal nails unit with 18 MHz linear transducer. Ital J Anat Embryol. 2009;114:137–44.
7. Wortsman X. Sonography of the nail. In: Wortsman X, Jemec GBE, editors. Dermatologic ultrasound with clinical and histologic correlations. New York: Springer; 2013. p. 419–76.
8. Wortsman X, Jemec GBE. Ultrasound imaging of nails. Dermatol Clin. 2006;24:323–8.
9. Thomas L, Vaudaine M, Wortsman X, Jemec GBE, Drapé JL. Imaging the nail unit. In: Baran R, de Berker D, Holzberg M, Thomas L, editors. Baran and Dawber's diseases of the nails and their management. 4th Chichester: Wiley-Blackwell; 2012. p. 132–153.
10. Wortsman X. Ultrasound in dermatology: why, how and when? Semin Ultrasound CT MR. 2013;34:177–95.
11. Wortsman X, Wortsman J, Matsuoka L, Saavedra T, Mardones F, Saavedra D, et al. Sonography in pathologies of scalp and hair. Br J Radiol. 2012;85:647–55.
12. Van Holsbeeck M, Introcaso J. Sonography of tendons. In: Van Holsbeeck M, Introcaso J, editors. Musculoskeletal ultrasound. 3rd ed. New Delhi: Jaypee Brothers Medical; 2016. p. 26–104.
13. Van Holsbeeck M, Introcaso J. Sonography of muscle. In: Van Holsbeeck M, Introcaso J, editors. Musculoskeletal ultrasound. 3d ed. New Delhi: Jaypee Brothers Medical; 2016. p. 105–187.
14. Van Holsbeeck M, Introcaso J. Sonography of bursae. In: Van Holsbeeck M, Introcaso J, editors. Musculoskeletal ultrasound. 3rd New Delhi: Jaypee Brothers Medical; 2016. p. 188–247.
15. Wortsman X, Jemec GBE. Ultrasound of the ear pinna. J Ultrasound Med. 2008;27:761–70.
16. Wortsman X, Azocar P. Wrist ultrasound. In: Dogra V, Gaitini D, editors. Musculoskeletal ultrasound with CT and MRI correlation. New York: Thieme; 2010. p. 46–70.
17. Wortsman X, Calderón P, Arellano J, Orellana Y. High-resolution color Doppler ultrasound of a caliber-persistent artery of the lip, a simulator variant of dermatologic disease: case report and sonographic findings. Int J Dermatol. 2009;48:830–3.
18. Arellano J, Antoniazzi C, Wortsman X. Early diagnosis of a caliber persistent labial artery in a child: usefulness of ultrasonography. Australas J Dermatol. 2012;53:e18–9.
19. Da Costa D, Taddese A, Cure ML, Gerson D, Poppiti R Jr, Esserman LE. Common and unusual diseases of the nipple-areolar complex. Radiographics. 2007;27(Suppl 1):S65–77.
20. Wortsman X, Claveria P, Valenzuela F, Molina MT, Wortsman J. Sonography of acne vulgaris. J Ultrasound Med. 2014;33:93–102.